Neuronal genetic rescue normalizes brain network dynamics in a lysosomal storage disorder despite persistent storage accumulation

Authors
Rebecca C. Ahrens-Nicklas*[1,2], Luis Tecedor[3], Arron F. Hall[2], Owen Kane[2], Richard J. Chung[2], Elena Lysenko[3], Eric D. Marsh[4,5], Colleen S. Stein[6], Beverly L. Davidson*[3,7]

Affiliations
[1]Department of Pediatrics, Perelman School of Medicine at the University of Pennsylvania.
[2]Division of Human Genetics, The Children's Hospital of Philadelphia.
[3]The Raymond G. Perelman Center for Cellular and Molecular Therapeutics, The Children's Hospital of Philadelphia.
[4]Department of Neurology, Perelman School of Medicine at the University of Pennsylvania.
[5]Division of Child Neurology, The Children's Hospital of Philadelphia.
[6]Department of Internal Medicine, Fraternal Order of Eagles Diabetes Research Center, Abboud Cardiovascular Research Center, Carver College of Medicine, University of Iowa.
[7]The Department of Pathology and Laboratory Medicine Perelman School of Medicine at the University of Pennsylvania.

*Correspondence should be addressed to co-corresponding authors

Rebecca C. Ahrens-Nicklas, MD, PhD
Children's Hospital of Philadelphia
3615 Civic Center Blvd Abramson 1016H
Philadelphia, PA 19104,
Tel: 215-590-3412
Email: ahrensnicklasr@email.chop.edu

AND

Beverly L. Davidson, PhD
Children's Hospital of Philadelphia,
3501 Civic Center Boulevard, 5060 CTRB,
Philadelphia, PA 19104,
Tel: 267-426-0929,
Email: davidsonbl@chop.edu

Short title: Genetic rescue of network activity in CLN3 Disease

Abstract

Although neurologic symptoms occur in two-thirds of lysosomal storage disorders (LSDs), for most we do not understand the mechanisms underlying brain dysfunction. A major unanswered question is if the pathogenic hallmark of LSDs, storage accumulation, induces functional defects directly or is a disease bystander. Also, for most LSDs we do not know the impact of loss-of-function in individual cell types. Understanding these critical questions are essential to therapy development. Here, we determined the impact of genetic rescue in distinct cell types on neural circuit dysfunction in CLN3 disease, the most common pediatric dementia and a representative LSD. We restored *Cln3* expression via AAV-mediated gene delivery and conditional genetic rescue in a CLN3 mouse model. Surprisingly, we found that low-level rescue of *Cln3* expression in neurons alone normalized clinically-relevant electrophysiologic markers of network dysfunction, despite the presence of substantial residual histopathology, in contrast to restoring expression in astrocytes. Thus, loss of Cln3 function in neurons, not storage accumulation, underlies neurologic dysfunction in CLN3 disease, implying that storage clearance may be an inappropriate target for therapy development and an ineffectual biomarker.

63 **Introduction**

64 Lysosomal storage disorders (LSDs) are a group of approximately 50 rare metabolic diseases
65 characterized by progressive accumulation of storage material in lysosomes. Neurological symptoms,
66 including neurocognitive regression, seizures, and psychiatric symptoms, occur in more than 2/3 of LSDs
67 and are generally not ameliorated by current therapies [1]. For many LSDs, including CLN3 disease, the
68 most common cause of childhood dementia, the mechanisms underlying neurologic dysfunction are
69 poorly understood.

70

71 The function of CLN3 protein remains unknown, hindering mechanism-based therapy development. The
72 brains of CLN3 disease mouse models demonstrate progressive storage accumulation, predominantly
73 comprised of subunit C of the mitochondrial ATP synthase (SCMAS) [2 3], mirroring what occurs in CLN3
74 disease patients[4]. Therefore, most drug development efforts rely on histopathologic markers of efficacy,
75 including reduction of storage material, reactive astrocytosis and microgliosis[2,4,5]. However, whether these
76 histopathologic changes cause disease, augment the disease process, or are simply harmless
77 epiphenomenon is unclear.

78

79 In addition to lack of clarity on the impact of storage, the role of various CNS cell types in driving
80 functional deficits in CLN3 disease is unknown. Astrocytes and microglia isolated from CLN3 disease
81 mouse models demonstrate altered cellular properties and physiology[6-8], and in animal models, localized
82 glial activation occurs in regions where neurons will later die[9] supporting a role for glia as a disease
83 driver. On the other hand, neurons from CLN3 animal models exhibit both histopathologic and functional
84 differences[2,10,11]. Ultimately, patients' symptoms such as seizures and neurologic regression arise directly
85 from functional changes in key neuronal circuits. Nonetheless, we do not understand what cell types
86 underlie these pathologic network dynamics in the brain.

87

88 Previously, we described network-level neurologic defects in both the cortex and hippocampus of two
89 CLN3 disease mouse models using *in vitro* voltage sensitive dye imaging and *in vivo* electrophysiology
90 techniques[12]. While many brain regions are affected in CLN3 disease, the cortex and hippocampus are
91 especially vulnerable and show early pathologic changes in mouse models and human patients[3,4,11,13].
92 We found that network-level changes begin early in the disease course before substantial storage
93 accumulation in both the hippocampus and cortex. In slice-recordings, these changes include
94 hypoexcitability of the dentate gyrus of the hippocampus, a region essential for learning and memory. On
95 *in vivo* electroencephalogram (EEG), CLN3 disease mice show frequent epileptiform spikes, a feature of
96 many epilepsy models, and a shift towards high frequency background activity, a change associated with
97 cognitive impairment and present in Alzheimer's disease models and patients[14,15].
98
99 To date, CLN3 disease research has been hindered by the fact that animal models have only subtle
100 behavioral and survival phenotypes[16,17]. Most manifest histopathologic changes including storage
101 accumulation and reactive astrocytosis; however, these phenotypes may not correlate with central nervous
102 system (CNS) dysfunction. Our network-level electrophysiologic approach provides a robust, clinically
103 meaningful measure of neurologic function that can probe disease mechanisms and evaluate potential
104 therapies.
105
106 Here, we developed a new 'conditional rescue' mouse model of CLN3 disease. The model is homozygous
107 for the most common human CLN3 disease mutation[2], but also carries a Cre-inducible wild-type *Cln3*
108 transgene, under the control of its endogenous promoter, allowing for cell-type specific rescue of
109 expression. We employed AAV-mediated gene replacement as a second strategy to restore *Cln3*
110 expression and combined these tools with network-level electrophysiology techniques to answer three
111 essential questions: 1) Does gene replacement correct neural circuit dysfunction in a LSD? 2) What cell
112 types must be corrected to improve network dynamics? and 3) Does storage accumulation underlie
113 deficits in CNS network dynamics in CLN3 disease?

114

115 **Results**

116 In prior work, we found that CLN3 disease mouse models demonstrate robust, progressive neuronal
117 network defects[12]. We first assessed if neonatal correction of most CNS cell types could prevent circuit-
118 level functional pathology. For this, we employed an adeno-associated virus serotype 9 (AAV9) vector
119 expressing wild-type murine *Cln3* under control of 1665 bp of the endogenous *Cln3* promoter, which
120 mimics the low levels of expression seen in the endogenous setting **(Sup Figure 1-2, Sup Methods).**
121 Vector was delivered at p0 via unilateral intracerebroventricular (ICV) injection into CLN3-deficient
122 mice to transduce both astrocytes and neurons[18] **(Sup Figure 3)**. The CLN3 disease mouse model harbors
123 the most common human CLN3 disease mutation, a deletion of exons 7 and 8 ($Cln3^{\Delta ex78/\Delta ex78}$) (*2*). ICV
124 injection of AAV9.CLN3 at a dose of $1e^{10}$ vg increased *Cln3* expression **(Figure 1A)**. One year after
125 injection, levels in the $Cln3^{\Delta ex78/\Delta ex78}$ hemisphere contralateral to the injection site reached 24.5% ± 4.7 of
126 heterozygous controls. When assessed histologically, gene replacement partially reduced storage
127 accumulation in both the hippocampus and motor cortex ipsilateral to the injection site **(Figure 1B, Sup**
128 **Figure 4**).

129

130 To determine the impact of p0 AAV9.CLN3 infusion on *in vivo* network dynamics, we recorded activity
131 throughout the brain via *in vivo* EEG. Twelve-month-old $Cln3^{\Delta ex78/\Delta ex78}$ mice have increased spike burden
132 and a shift in background activity towards faster frequencies, with increased power in faster frequency
133 bands, as compared to $Cln3^{\Delta ex78/WT}$ controls **(Figure 1C-D)**. Specifically, there is decreased power in the
134 slow delta frequency band (0.1-4Hz) and a trend towards increased power in the faster beta (13-25Hz)
135 and gamma (25-50Hz) bands in $Cln3^{\Delta ex78/\Delta ex78}$ mice, consistent with our previous report in *Cln3* knock-out
136 mice[12]. Remarkably, restoring gene expression at p0 normalized spiking rates **(Figure 1C)** and corrected
137 background activity **(Figure 1D)** in 12-month-old $Cln3^{\Delta ex78/\Delta ex78}$ AAV9.CLN3-treated animals. Correction

138 of EEG phenotypes was equally effective in both the hemispheres. Thus, early gene replacement can
139 normalize network dynamics, and this rescue does not require full inhibition of storage accumulation.
140
141 Because AAV9 delivered to neonates transduces astrocytes and neurons[18], it is unclear whether all cell
142 types must be corrected to improve circuit function, a question critically important to translate gene
143 therapies to children. AAV9 delivered into the CNS generally transduces neurons in adult mice and
144 juvenile and adult large animal models[19-21]. To address this, we developed a conditional rescue model of
145 CLN3 disease, the Flex*Cln3* mouse. This model is homozygous for the common *Cln3* exon 7-8 deletion
146 and also carries the Cre-inducible Flex*Cln3* allele, permitting expression of wild-type Cln3 protein in the
147 presence of Cre recombinase **(Figure 2, Sup Methods and Sup Figures 5-7)**. The Flex*Cln3* allele is
148 under control of the same 1665 bp *Cln3* promoter as used for AAV-mediated gene replacement.
149
150 We validated the model by crossing Flex*Cln3* mice with *Zp3-Cre* mice[22] to drive germline level
151 recombination and flip the reverse-oriented wildtype Flex*Cln3* allele into the forward orientation in all
152 cells. Recombination of the allele was confirmed using orientation-specific PCR primers on genomic
153 DNA extracted from the hippocampus **(Figure 2B, Sup Figure 7)**. In these mice *Cln3* expression was
154 ubiquitously restored, with expression levels dictated by the transgenic *Cln3* 1665 bp promoter. *Cln3*
155 expression in the hippocampus was restored to 40% of heterozygous ($Cln3^{\Delta ex78/WT}$) control levels as
156 determined by qPCR **(Figure 2C)**. Correction (i.e. expression of the Flex*Cln3* transgene) in all cell types
157 (Flex*Cln3*/ $Cln3^{\Delta ex78/\Delta ex78}$/ *Zp3*-Cre) substantially reduced SCMAS storage in the hippocampus and other
158 brain regions **(Figure 2D, Sup Figure 8)**.
159
160 For selective rescue of astrocytes or neurons, Flex*Cln3* mice were crossed to *Gfap*-Cre[23] or *Syn1*-Cre[24]
161 driver lines, respectively. Cre-mediated rearrangement of the Flex*Cln3* allele was confirmed by PCR of
162 genomic DNA extracted from the hippocampus using orientation specific primers **(Figure 3A)**. As Cre is

163 only expressed in a subset of cells (either astrocytes or neurons), unlike in the case of *Zp3*-Cre **(Figure**
164 **2B)**, both the forward and reverse alleles were detected in hippocampal tissue.
165
166 Expression of forward-oriented Flex*Cln3* transcripts was confirmed in the hippocampus of the astrocyte
167 and neuronal-specific rescue models. As rescue did not occur in all cell types, and Cln3 protomer activity
168 and expression can vary between cells and be induced by disease pathology[3] it is difficult to normalize
169 expression levels to heterozygote controls. However, to get a relative sense of expression levels we
170 compared the level of Flex*Cln3* transgene expression in the astrocyte-only and neuron-only rescue
171 models. We found no differences in transcript levels (normalized ΔCT values of 14.1 vs. 13.4, p=0.53 by
172 unpaired t-test) between the groups **(Figure 3B)**. As there are no available antibodies that can reliably
173 detect endogenous levels of mouse Cln3 protein[25], we could not assess protein expression.
174
175 We next determined the impact of cell type-selective restoration of *Cln3* on histopathological readouts.
176 Rescue of *Cln3* expression in either astrocytes (Flex*Cln3* / *Cln3*$^{\Delta ex78/\Delta ex78}$ / *Gfap*-Cre) or neurons
177 (Flex*Cln3* / *Cln3*$^{\Delta ex78/\Delta ex78}$ / *Syn1*-Cre) alone did not prevent storage accumulation in the hippocampus or
178 motor cortex in 6 or 12-month-old mice **(Figure 3C-L, Sup Figures 8-9)**. In addition to storage
179 accumulation, CLN3 disease mice develop progressive, reactive astrocytosis. At twelve months of age,
180 both the hippocampus and motor cortex of *Cln3*$^{\Delta ex78/\Delta ex78}$ showed increased astrocytosis as compared to
181 wild-type controls. Rescue of *Cln3* expression in either neurons or astrocytes alone did not prevent
182 astrocytosis **(Sup Figure 10)**.
183
184 To investigate if the Flex*Cln3* transgene could prevent storage accumulation in the specific cell type
185 where it was expressed, we investigated co-localization of autofluorescent lipofuscin with a neuronal
186 marker, NeuN, in cortical tissue **(Figure 4)**. There is little lipofuscin accumulation in *Cln3*$^{WT/WT}$ cortex
187 **(Figure 4, top row)**, as compared to *Cln3*$^{\Delta ex78/\Delta ex78}$ cortex, where there is storage in both neurons and non-
188 neuronal cells (**Figure 4, second row)**. Ubiquitous Flex*Cln3* allele expression (in the presence of *Zp3*-

189 Cre) prevented storage accumulation in all cell types **(Figure 4, third row)**. Flex*Cln3* allele expression
190 in neurons (in the presence of *Syn1*-Cre) did not prevent storage in either neurons or non-neuronal cells
191 **(Figure 4, bottom row)**.
192
193 Next, we determined if restoring *Cln3* expression could improve electrophysiologic measures, despite
194 residual storage accumulation. *In vitro* voltage sensitive dye imaging of hippocampal slices from 6-
195 month-old animals was completed in Flex*Cln3* / *Cln3*$^{\Delta ex78/\Delta ex78}$ / *Gfap*-Cre, Flex*Cln3* / *Cln3*$^{\Delta ex78/\Delta ex78}$ /
196 *Syn1*-Cre*, and* Flex*Cln/Cln3*$^{\Delta ex78/\Delta ex78}$ /Zp3 mice. In this early-stage of disease, the internal blade of the
197 dentate gyrus of the *Cln3*$^{\Delta ex78/\Delta ex78}$ hippocampus was hypoexcitable in response to perforant path
198 stimulation as compared to heterozygous *Cln3*$^{\Delta 78/WT}$ mice **(Figure 5A-C)**, consistent with our previous
199 studies[12]. Specifically, 32.7% of pixels in the internal blade of the *Cln3*$^{\Delta ex78/\Delta ex78}$ dentate gyrus were
200 significantly hypoexcitable as compared to slices obtained from heterozygous control animals.
201 Interestingly, restoring expression in astrocytes did not correct hypoexcitability of the dentate gyrus
202 **(Figure 5D-E)**. However, restoring *Cln3* expression in neurons was sufficient to prevent disease-induced
203 hypoexcitability **(Figure 5F-G)**, in fact excitability was mildly increased as compared to controls. This
204 rescue of dynamics occurred despite the presence of residual histopathology **(Figure 3-4 and Sup.**
205 **Figures 8-10)**.
206
207 To evaluate how cell-type specific correction modulates CNS functional defects *in vivo,* we measured
208 network activity through long-term EEG recordings. While restoration of *Cln3* expression in either
209 astrocytes or neurons prevented epileptiform spikes throughout the brain (**Figure 6A**), only rescue in
210 neurons corrected EEG background frequency composition (i.e. frequency band power) and thereby fully
211 normalized network activity **(Figure 6B-C)**. Intriguingly, this correction of physiology occurred despite
212 the presence of substantial storage burden, revealing for the first time that loss of Cln3 protein function in
213 neurons, not storage burden, underlies functional defects in CLN3 disease.
214

215 **Discussion**

216 Previous cellular-level studies of CLN3 disease have demonstrated disease-associated abnormalities in
217 both neurons and astrocytes[4,7-9,11,26-28]. Prior to this work, it was unknown how these cellular defects
218 translate to the circuit-level dysfunction that underlies neurological symptoms such as dementia and
219 seizures that CLN3 disease patients experience. This work highlights the fact that neurons underlie
220 functional defects in CLN3 disease and must be targeted in future drug development efforts.
221
222 A number of novel therapies, including small molecule[5,29-33], antisense oligonucleotides[34], and gene
223 replacement [35,36] strategies are under development for CLN3 disease. These approaches will not target all
224 cell types equally. For example, studies in non-human primates have demonstrated that intravenous
225 administration of AAV9 in juvenile non-human primates predominately transduces glia[21,37] while direct
226 administration into the cerebral spinal fluid (CSF) improves delivery to neurons[38] (34). Our results
227 suggest that maximizing neuronal correction will be essential to develop a treatment that improves
228 functional outcomes in CLN3 disease.
229
230 In previous studies, *Cln3*$^{\Delta ex78/\Delta ex78}$ mice have demonstrated abnormal astrocytic-neuronal coupling[7].
231 Monogenic mouse models of isolated astrocyte dysfunction have epileptiform spikes and seizures on EEG
232 because of pathologic cross-talk between astrocytes and neurons[39]. In the Flex*Cln3* mouse, while rescue
233 of *Cln3* expression in astrocytes did not normalize EEG background, it was sufficient to prevent
234 epileptiform spikes. The reduction in spiking likely reflects improved astrocytic-neuronal interactions
235 when *Cln3* expression is restored in astrocytes. Collectively, our data suggests that diseased astrocytes
236 may modulate network-level dysfunction in CLN3 disease, but diseased neurons are the primary driver of
237 functional deficits.
238
239 Using our cell-type specific rescue model, we found that storage accumulation was prevented when *Cln3*
240 was reintroduced to all cell types embryonically, but not when that correction was restricted to astrocytes

or neurons alone. Interestingly, prevention of storage accumulation is not required for correcting neuronal network physiology, suggesting that storage material does not underlie functional defects and may be an innocent bystander in the disease process. These studies highlight the importance of using clinically-relevant functional measures, such as *in vivo* electrophysiology studies, to guide treatment development. Histologic measures, such as storage burden, may be poor surrogate biomarkers of therapeutic efficacy in CLN3 disease and possibly other neuronopathic LSDs.

In summary, partial restoration of Cln3 expression by AAV vectors or through Cre-based systems shows that neuronal expression is critical for preventing deficits in CNS functional circuits in CLN3 disease mice. This work also highlights that improvement in storage burden may be a poor readout of therapeutic efficacy in CLN3 disease, a phenomenon that should be considered by the broader LSD community.

Materials and Methods

For additional information, see Supplemental Methods.

Study approval: All animal protocols were approved by the Institutional Animal Care and Use Committee at the Children's Hospital of Philadelphia.

Statistical Analysis: All statistical analysis of VSDI rasters was completed using a permutation sampling method and the VSDI toolbox in MATLAB (Mathworks) as previously described[12,40]. For summary statistics of regions or groups, GraphPad Prism was also used. In graphs, data are expressed as mean ± SEM. The statistical significance of the observed differences between 2 groups was assessed by two-tailed t-test (for normally distributed data) or Mann-Whitney U test (for non-normally distributed data). For grouped data sets that were not normally distributed a Kruskal-Wallis test followed by a multiple comparisons test was used as detailed in each figure legend. For grouped data sets that were normally distributed, 1-way ANOVA or 2-way ANOVA followed by multiple-comparisons test was completed as

267 detailed in each figure legend. Results were considered significant when $p < 0.05$. Male and female mice
268 were included in all groups.
269
270
271 **Acknowledgments:** NINDS R21NS084424 and NICHD HD33532 to BLD, NIH K08NS105865 to RAN,
272 NCL Stiftung Research Award to RAN, Children's Hospital of Philadelphia Research Institute support to
273 RAN and BLD.
274
275 **Conflicts of interests:** BLD is a founder of Spark Therapeutics and Spirovant is on the scientific advisory
276 boards of Intellia Therapeutics, Homology Medicines, Prevail Therapeutics, Resilience, Moment Bio,
277 Spirovant, Saliogen and Panorama Medicines. No other authors report conflicts of interest.
278
279
280 **Author contributions:**
281 Design of study: RA, LT, AH, OK, RC, EL, EM, CS, BD
282 Data acquisition and analysis of data: RA, LT, AH, OK, RC, EL, CS
283 Drafting of manuscript: RA, LT, AH, OK, CS
284 Critical review of data and manuscript: RA, LT, EM, CS, BD

Figures

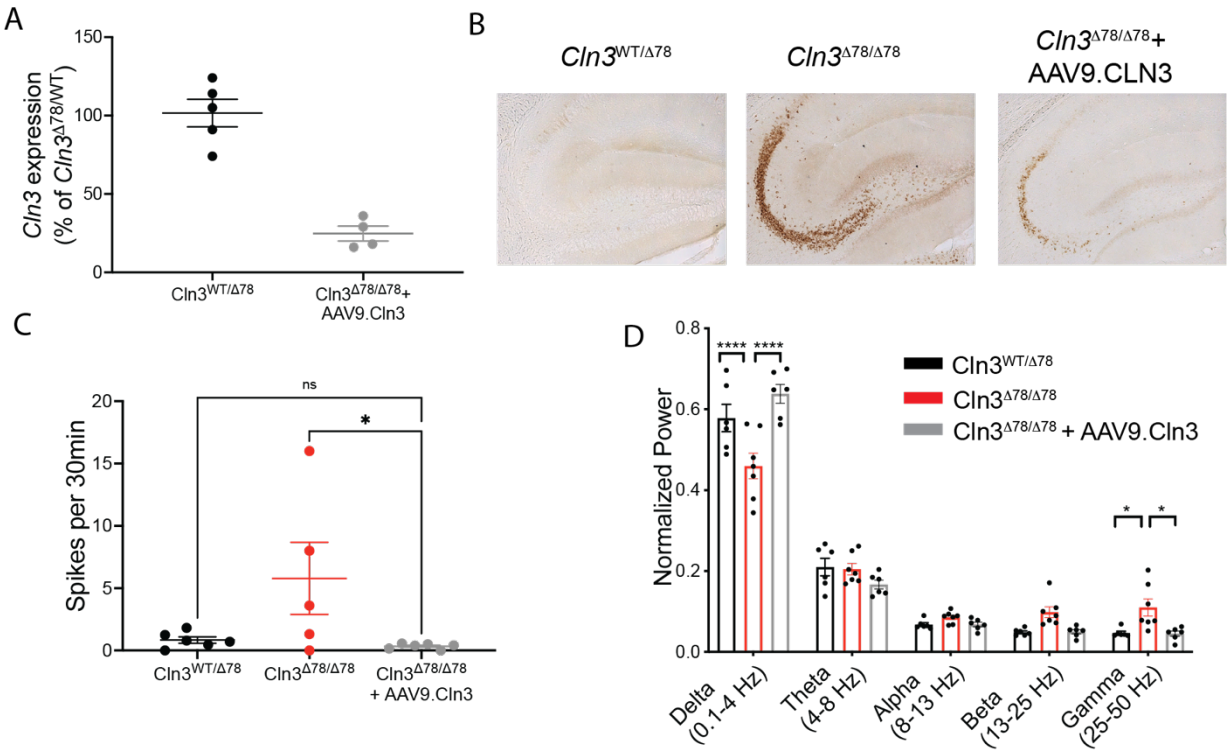

Figure 1: Intracerebroventricular AAV9.CLN3 gene therapy given at p0 normalizes neuronal network dynamics *in vivo* at 12 months of age. (A) p0 ICV injection of AAV9.Cln3 restored Cln3 expression in *Cln3*$^{\Delta ex78/\Delta ex78}$ mouse brain at 12 months of age, with levels in the *Cln3*$^{\Delta ex78/\Delta ex78}$ hemisphere contralateral to the injection site reaching 24.5% ± 4.7 of heterozygous controls. **(B)** Subunit C of the mitochondrial ATP synthase (SCMAS) accumulation is partially corrected in the hippocampus ipsilateral to the injection site of *Cln3*$^{\Delta ex78/\Delta ex78}$ mice treated with AAV9.CLN3. Gene replacement corrects circuit function measured on intracranial EEG including **(C)** epileptiform spiking rates throughout the cortex (average of all cortical leads shown) and **(D)** background frequency band composition in the motor cortex. Groups: *Cln3*$^{WT/\Delta ex78}$ (black); *Cln3*$^{\Delta ex78/\Delta ex78}$ (red); *Cln3*$^{\Delta ex78/\Delta ex78}$ + AAV9.CLN3 (gray). N=5-6 animals/condition. Results from 12 hours of recordings were averaged for each animal shown as an individual circle. Spikes analyzed using a non-parametric Kruskal-Wallis test followed by Dunn's multiple comparisons test. Frequency bands were analyzed by two-way ANOVA by band and genotype,

299 followed by Bonferonni's multiple comparisons test (significant results of multiple comparison testing

300 shown as *p<0.05, **p<0.01, ***p<0.001, ****p<0.0001). Data are shown as mean +/- s.e.m.

301

302

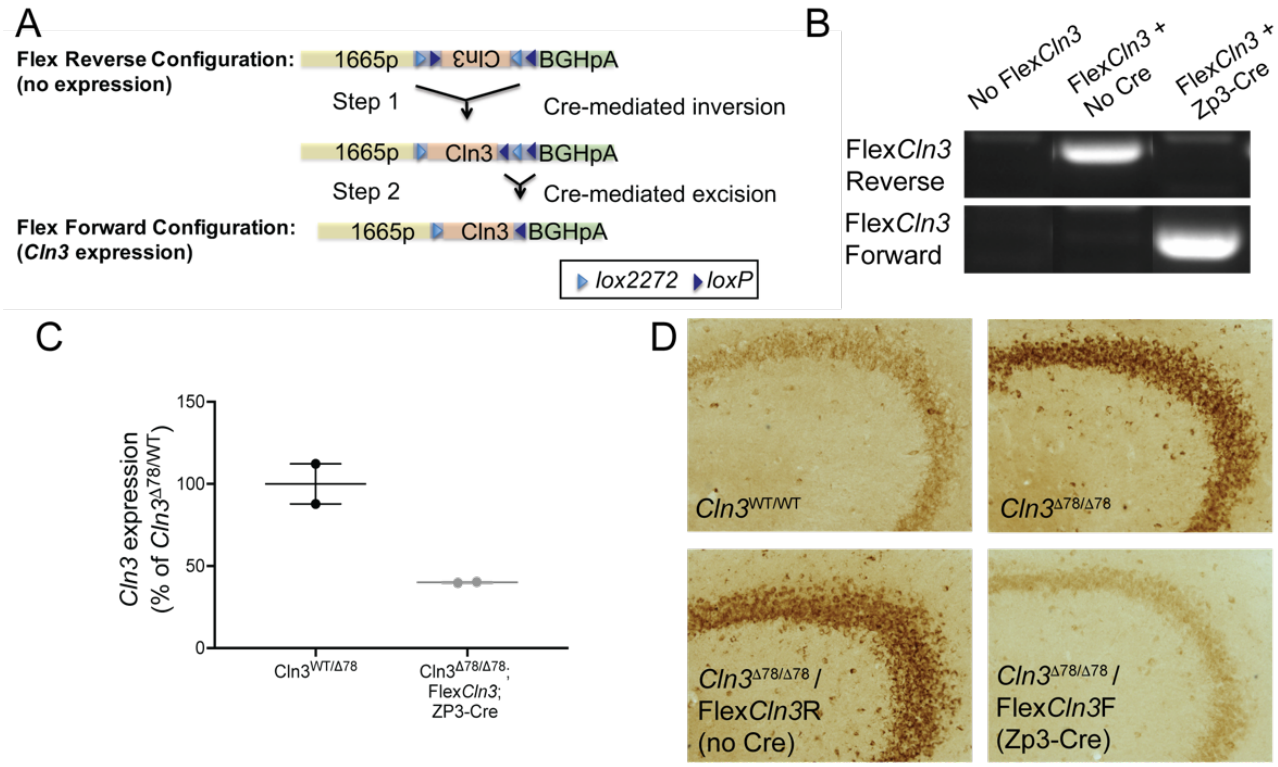

Figure 2: Expression of Flex*Cln3* allele in all cells reduces storage accumulation in *Cln3*$^{\Delta ex78/\Delta ex78}$ brain. (A) In the presence of Cre, the Flex*Cln3* allele undergoes inversion (Step 1) and excision (Step 2) and is expressed under control of its endogenous promoter. **(B)** PCR of genomic DNA from hippocampus using orientation-specific primers confirms that the Flex*Cln3* is in the forward orientation only in the presence of Cre (see Sup Figure 7 for uncut gels). **(C)** In the presence of *Zp3*-Cre which drives ubiquitous recombination, the Flex*Cln3* allele results in expression levels that are 40.0 +/- 0.4% of heterozygous controls. **(D)** Subunit C of the mitochondrial ATP synthase (SCMAS) accumulates in the hippocampus of *Cln3*$^{\Delta ex78/\Delta ex78}$ and Flex*Cln3* / *Cln3*$^{\Delta ex78/\Delta ex78}$ mice. Storage is reduced in mice with the Flex*Cln3* allele in the forward confirmation.

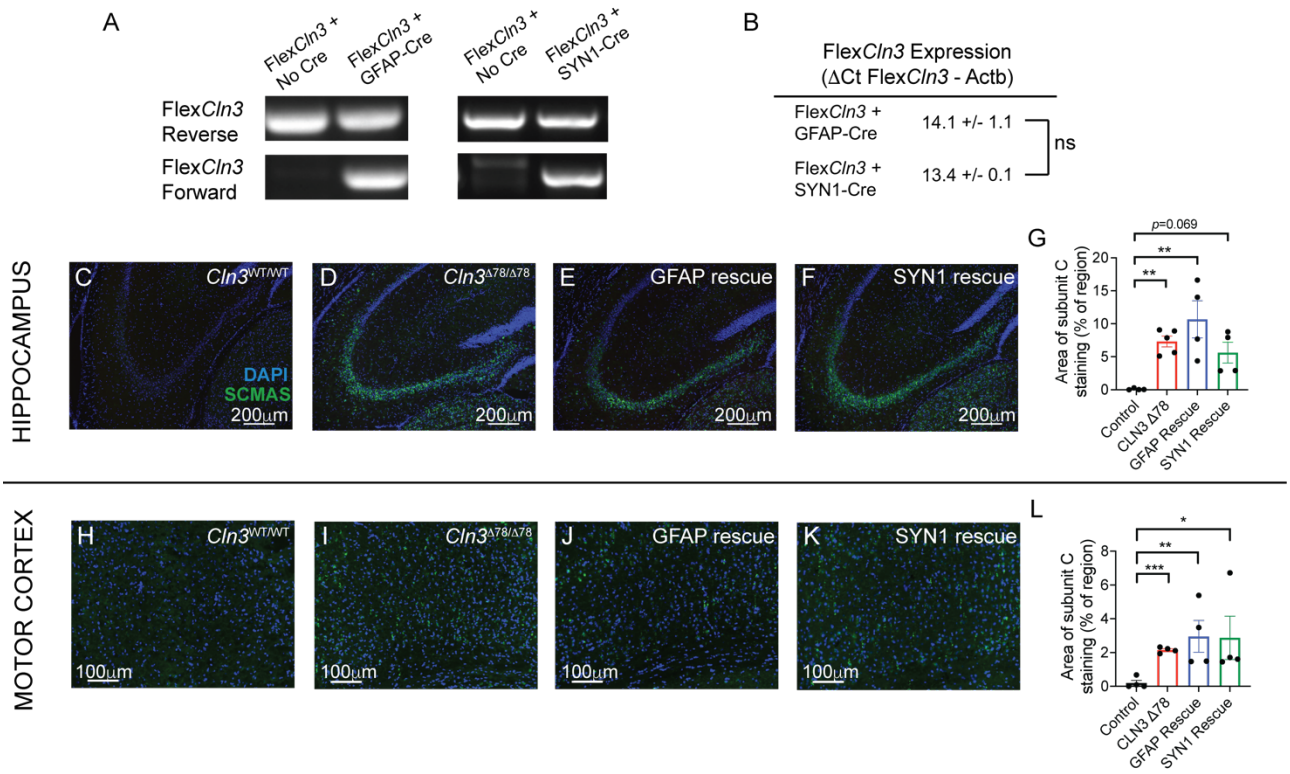

Figure 3: Expression of Flex*Cln3* allele in either neurons or astrocytes alone does not prevent storage accumulation. (A) In the presence of Cre, the Flex*Cln3* allele undergoes inversion as detected by PCR with orientation-specific primers of genomic DNA from hippocampus. As both the *Gfap*-Cre and *Syn1*-Cre only drive recombination in a subset of cells, both the forward and reverse alleles are detected (see Sup Figure 7 for uncut gels). **(B)** Expression levels as measured by ΔCt values (FlexCln3-βactin) are similar in Flex*Cln3* brain in the presence of *Gfap*-Cre and *Syn1*-Cre (14.1 vs. 13.4, p=0.53 by unpaired t-test). **(C-G)** Expression of Flex*Cln3* in astrocytes (Flex*Cln3* / *Cln3*$^{\Delta ex78/\Delta ex78}$ / *Gfap*-Cre animals) or neurons alone (Flex*Cln3* / *Cln3*$^{\Delta ex78/\Delta ex78}$ / *Syn1*-Cre animals) does not prevent accumulation of SCMAS (green). **(H-K)** Similar findings were seen in the motor cortex. N=4-5 animals, non-parametric Kruskal-

330 Wallis test followed by Benjamini and Hochberg multiple comparisons correction to detect differences

331 from control. For all panels: *p<0.05, **p<0.01, ***p<0.001, ****p<0.0001.

332

333

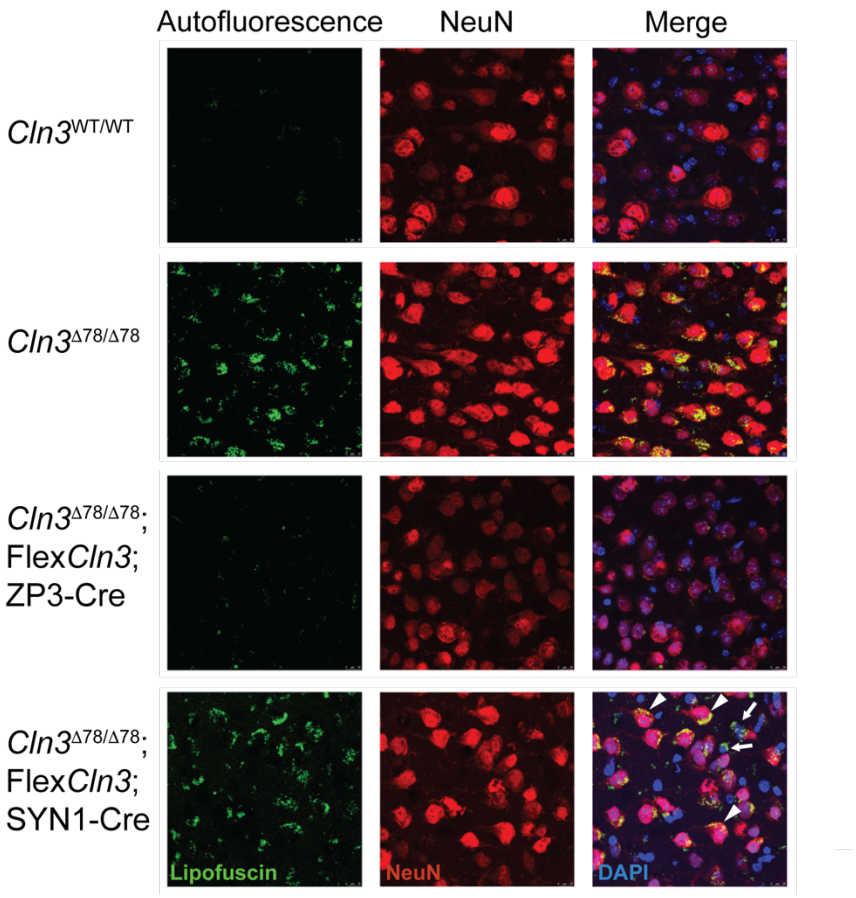

334

335

336 **Figure 4: Expression of the Flex*Cln3* allele in neurons alone does not prevent autofluorescent**

337 **lipofuscin accumulation in cortical neurons. (Top row)** There is little autofluorescent lipofuscin

338 accumulation (green) in wild-type cortical neurons (red) (blue DAPI) as compared to **(second row)**

339 *Cln3*$^{\Delta 78/\Delta 78}$ cortical neurons in 12 month old animals. **(Third row)** *Zp3*-Cre induced expression of the

340 Flex*Cln3* allele in all cell types prevents autofluorescent lipofuscin accumulation in both neuronal and

341 non-neuronal cells. **(Bottom row)** Flex*Cln3* expression in neurons (*Syn1*-Cre) did not prevent storage

342 accumulation in neurons (arrow heads) or non-neuronal cells (arrows).

343

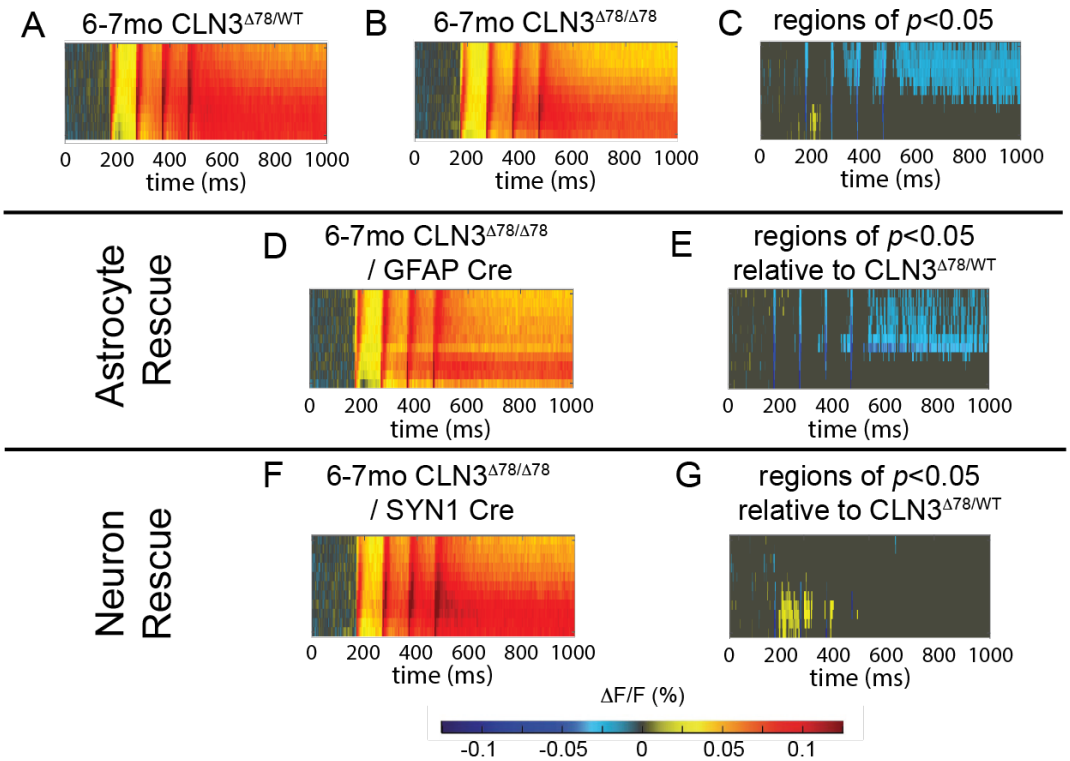

Figure 5: Restoring low level *Cln3* expression in neurons alone corrects hypoexcitability of the dentate gyrus. Dentate gyrus excitability measured through *in vitro* voltage sensitive dye imaging of hippocampal slices from 6-month-old animals is shown as raster plots of average fluorescence change (ΔF/F warm colors excitation, cool colors inhibition) over time (X axis) and location within the internal blade of the dentate gyrus (Y Axis). **(A)** Four-pulse stimulation of the perforant path in heterozygous control ($Cln3^{\Delta ex78/WT}$) mice reveals robust excitation of the dentate gyrus (DG) as compared to **(B)** $Cln3^{\Delta ex78/\Delta ex78}$ mice**. (C)** $Cln3^{\Delta ex78/WT}$ vs. $Cln3^{\Delta ex78/\Delta ex78}$ rasters were compared using a permutation sampling method with 1000 trials. Pixels with $p>0.05$ are masked in gray. For regions of significant difference in excitability with $p<0.05$, the difference in fluorescence change ($\Delta F/F_{\Delta ex78/WT}$ -$\Delta F/F_{\Delta ex78/\Delta ex78}$) is shown. **(D-E)** In animals expressing *Cln3* in astrocytes (Flex*Cln3* / $Cln3^{\Delta ex78/\Delta ex78}$ / *Gfap*-Cre), the DG remained hypoexcitable as compared to the $Cln3^{\Delta ex78/WT}$ DG. **(F-G)** Expression of *Cln3* in neurons alone (Flex*Cln3* / $Cln3^{\Delta ex78/\Delta ex78}$ / *Syn1*-Cre) was sufficient to reverse hypoexcitability of the DG as compared to

358 *Cln3*$^{\Delta ex78/WT}$ animals. Group sizes (n=slices, N=mice): *Cln3*$^{\Delta ex78/WT}$ n= 23 N=4; *Cln3*$^{\Delta ex78/\Delta ex78}$ n= 30, N=6;

359 Flex*Cln3* / *Cln3*$^{\Delta ex78/\Delta ex78}$ / *Gfap-Cre* n=19 slices, N=4; Flex*Cln3* / *Cln3*$^{\Delta ex78/\Delta ex78}$ / *Syn1-Cre* n=17; N=4.

360

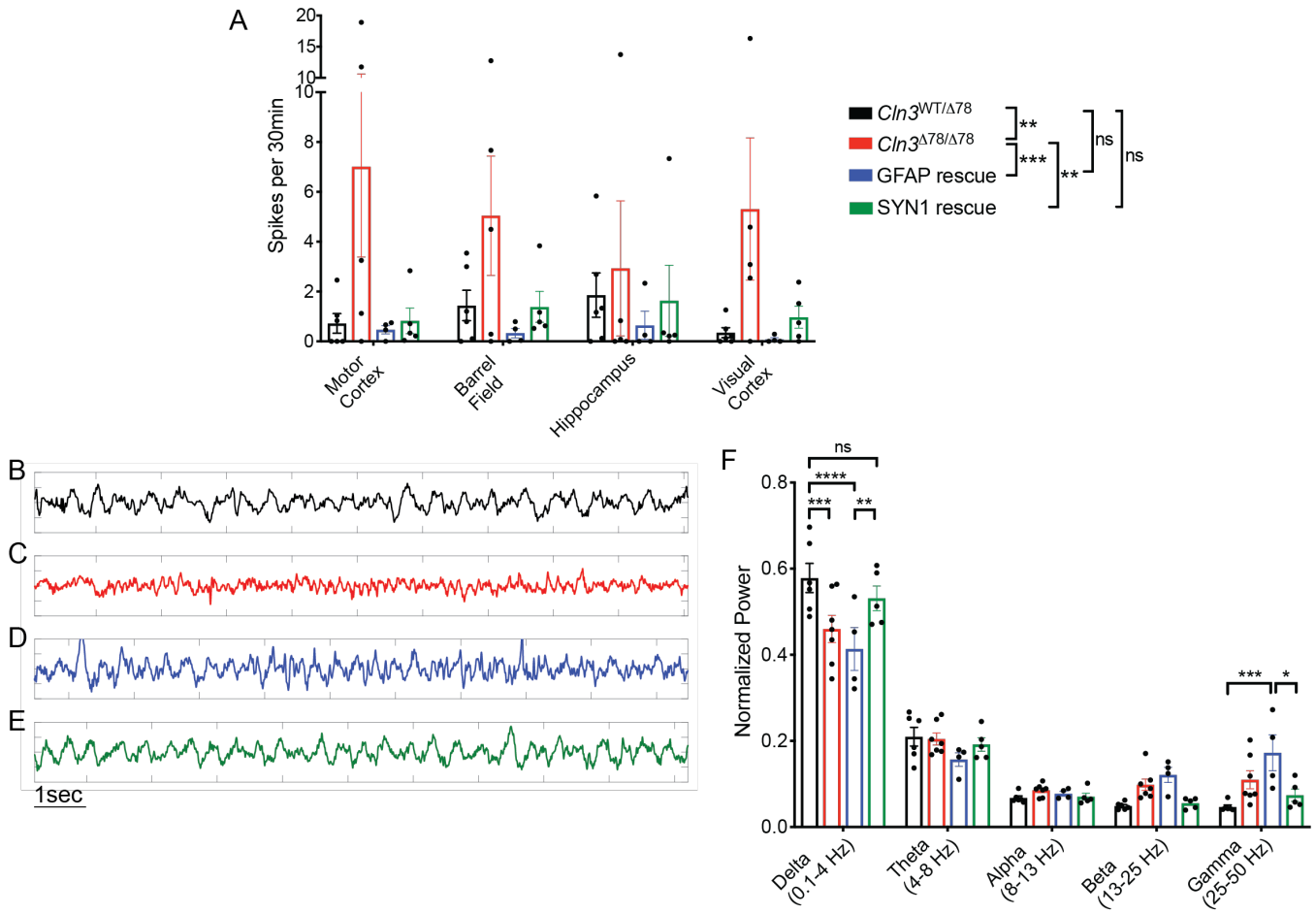

Figure 6: Cln3 rescue in either astrocytes or neurons reduces epileptiform spikes, but only neuronal rescue fully normalizes network dynamics as measured on EEG. (A) Correction of either astroctyes (Flex*Cln3* / *Cln3*$^{\Delta ex78/\Delta ex78}$ / *Gfap*-Cre, blue) or neurons (Flex*Cln3* / *Cln3*$^{\Delta ex78/\Delta ex78}$ / *Syn1*-Cre, green) reduced spike burden on EEG in 12 month old mice. **(B-E)** Example EEG traces from *Cln3*$^{\Delta ex78/\Delta ex78}$ (red) and Flex*Cln3* / *Cln3*$^{\Delta ex78/\Delta ex78}$ / *Gfap*-Cre motor cortex (blue) show decreased slow delta activity and increased fast activity as compared to control motor cortex (black). EEG trace from Flex*Cln3* / *Cln3*$^{\Delta ex78/\Delta ex78}$ / *Syn1*-Cre motor cortex (green) shows that rescue of *Cln3* expression in neurons normalizes EEG background frequency composition. **(F)** Power spectral analysis of EEG data recorded in the motor cortex confirms that rescue of *Cln3* expression in astrocytes (blue) does not correct disease-associated loss of delta activity, and actually exacerbates increased fast gamma activity. However, correction in

373 neurons (green) normalizes EEG frequency composition. N=4-5 animals/genotype, after passing a
374 Shapiro-Wilk test of normality, data were analyzed by two-way ANOVA, followed by Sidak's multiple
375 comparisons test. Significant differences from multiple comparisons testing are shown as *$p<0.05$,
376 **$p<0.01$, ***$p<0.001$. Frequency data in panel F in *Cln3*$^{WT/\Delta ex78}$ and *Cln3*$^{\Delta ex78/\Delta ex78}$ also shown in Fig 1D.
377
378
379
380

References

1. Platt, F.M. (2018). Emptying the stores: lysosomal diseases and therapeutic strategies. Nat Rev Drug Discov *17*, 133-150. 10.1038/nrd.2017.214.
2. Cotman, S.L., Vrbanac, V., Lebel, L.A., Lee, R.L., Johnson, K.A., Donahue, L.R., Teed, A.M., Antonellis, K., Bronson, R.T., Lerner, T.J., and MacDonald, M.E. (2002). Cln3(Deltaex7/8) knock-in mice with the common JNCL mutation exhibit progressive neurologic disease that begins before birth. Hum Mol Genet *11*, 2709-2721. 10.1093/hmg/11.22.2709.
3. Eliason, S.L., Stein, C.S., Mao, Q., Tecedor, L., Ding, S.L., Gaines, D.M., and Davidson, B.L. (2007). A knock-in reporter model of Batten disease. J Neurosci *27*, 9826-9834. 10.1523/JNEUROSCI.1710-07.2007.
4. Tyynela, J., Cooper, J.D., Khan, M.N., Shemilts, S.J., and Haltia, M. (2004). Hippocampal pathology in the human neuronal ceroid-lipofuscinoses: distinct patterns of storage deposition, neurodegeneration and glial activation. Brain Pathol *14*, 349-357. 10.1111/j.1750-3639.2004.tb00077.x.
5. Tarczyluk-Wells, M.A., Salzlechner, C., Najafi, A.R., Lim, M.J., Smith, D., Platt, F.M., Williams, B.P., and Cooper, J.D. (2019). Combined Anti-inflammatory and Neuroprotective Treatments Have the Potential to Impact Disease Phenotypes in Cln3 (-/-) Mice. Front Neurol *10*, 963. 10.3389/fneur.2019.00963.
6. Xiong, J., and Kielian, T. (2013). Microglia in juvenile neuronal ceroid lipofuscinosis are primed toward a pro-inflammatory phenotype. J Neurochem *127*, 245-258. 10.1111/jnc.12385.
7. Burkovetskaya, M., Karpuk, N., Xiong, J., Bosch, M., Boska, M.D., Takeuchi, H., Suzumura, A., and Kielian, T. (2014). Evidence for aberrant astrocyte hemichannel activity in Juvenile Neuronal Ceroid Lipofuscinosis (JNCL). PLoS One *9*, e95023. 10.1371/journal.pone.0095023.
8. Parviainen, L., Dihanich, S., Anderson, G.W., Wong, A.M., Brooks, H.R., Abeti, R., Rezaie, P., Lalli, G., Pope, S., Heales, S.J., Mitchison, H.M., et al. (2017). Glial cells are functionally impaired in juvenile neuronal ceroid lipofuscinosis and detrimental to neurons. Acta Neuropathol Commun *5*, 74. 10.1186/s40478-017-0476-y.
9. Pontikis, C.C., Cella, C.V., Parihar, N., Lim, M.J., Chakrabarti, S., Mitchison, H.M., Mobley, W.C., Rezaie, P., Pearce, D.A., and Cooper, J.D. (2004). Late onset neurodegeneration in the Cln3-/- mouse model of juvenile neuronal ceroid lipofuscinosis is preceded by low level glial activation. Brain Res *1023*, 231-242. 10.1016/j.brainres.2004.07.030.
10. Brenneman, D.E., Pearce, D.A., Kovacs, A., and DeFrees, S. (2017). Pharmacological Effects on Ceroid Lipofuscin and Neuronal Structure in Cln3 (ex7/8) Mouse Brain Cultures. J Mol Neurosci *63*, 100-114. 10.1007/s12031-017-0962-5.
11. Grunewald, B., Lange, M.D., Werner, C., O'Leary, A., Weishaupt, A., Popp, S., Pearce, D.A., Wiendl, H., Reif, A., Pape, H.C., Toyka, K.V., et al. (2017). Defective synaptic transmission causes disease signs in a mouse model of juvenile neuronal ceroid lipofuscinosis. Elife *6*. 10.7554/eLife.28685.
12. Ahrens-Nicklas, R.C., Tecedor, L., Hall, A.F., Lysenko, E., Cohen, A.S., Davidson, B.L., and Marsh, E.D. (2019). Neuronal network dysfunction precedes storage and neurodegeneration in a lysosomal storage disorder. JCI Insight *4*. 10.1172/jci.insight.131961.

427 13. Mitchison, H.M., Lim, M.J., and Cooper, J.D. (2004). Selectivity and types of cell death
428 in the neuronal ceroid lipofuscinoses. Brain Pathol *14*, 86-96. 10.1111/j.1750-
429 3639.2004.tb00502.x.
430 14. Kwak, Y.T. (2006). Quantitative EEG findings in different stages of Alzheimer's disease.
431 J Clin Neurophysiol *23*, 456-461. 10.1097/01.wnp.0000223453.47663.63.
432 15. Kent, B.A., Strittmatter, S.M., and Nygaard, H.B. (2018). Sleep and EEG Power Spectral
433 Analysis in Three Transgenic Mouse Models of Alzheimer's Disease: APP/PS1,
434 3xTgAD, and Tg2576. J Alzheimers Dis *64*, 1325-1336. 10.3233/JAD-180260.
435 16. Faller, K.M., Gutierrez-Quintana, R., Mohammed, A., Rahim, A.A., Tuxworth, R.I.,
436 Wager, K., and Bond, M. (2015). The neuronal ceroid lipofuscinoses: Opportunities from
437 model systems. Biochim Biophys Acta *1852*, 2267-2278. 10.1016/j.bbadis.2015.04.022.
438 17. Johnson, T.B., Langin, L.M., Zhao, J., Weimer, J.M., Pearce, D.A., and Kovacs, A.D.
439 (2019). Changes in motor behavior, neuropathology, and gut microbiota of a Batten
440 disease mouse model following administration of acidified drinking water. Sci Rep *9*,
441 14962. 10.1038/s41598-019-51488-z.
442 18. Hammond, S.L., Leek, A.N., Richman, E.H., and Tjalkens, R.B. (2017). Cellular
443 selectivity of AAV serotypes for gene delivery in neurons and astrocytes by neonatal
444 intracerebroventricular injection. PLoS One *12*, e0188830.
445 10.1371/journal.pone.0188830.
446 19. Hinderer, C., Bell, P., Vite, C.H., Louboutin, J.P., Grant, R., Bote, E., Yu, H., Pukenas,
447 B., Hurst, R., and Wilson, J.M. (2014). Widespread gene transfer in the central nervous
448 system of cynomolgus macaques following delivery of AAV9 into the cisterna magna.
449 Mol Ther Methods Clin Dev *1*, 14051. 10.1038/mtm.2014.51.
450 20. Gray, S.J., Nagabhushan Kalburgi, S., McCown, T.J., and Jude Samulski, R. (2013).
451 Global CNS gene delivery and evasion of anti-AAV-neutralizing antibodies by
452 intrathecal AAV administration in non-human primates. Gene Ther *20*, 450-459.
453 10.1038/gt.2012.101.
454 21. Samaranch, L., Salegio, E.A., San Sebastian, W., Kells, A.P., Foust, K.D., Bringas, J.R.,
455 Lamarre, C., Forsayeth, J., Kaspar, B.K., and Bankiewicz, K.S. (2012). Adeno-associated
456 virus serotype 9 transduction in the central nervous system of nonhuman primates. Hum
457 Gene Ther *23*, 382-389. 10.1089/hum.2011.200.
458 22. Shafi, R., Iyer, S.P., Ellies, L.G., O'Donnell, N., Marek, K.W., Chui, D., Hart, G.W., and
459 Marth, J.D. (2000). The O-GlcNAc transferase gene resides on the X chromosome and is
460 essential for embryonic stem cell viability and mouse ontogeny. Proc Natl Acad Sci U S
461 A *97*, 5735-5739. 10.1073/pnas.100471497.
462 23. Gregorian, C., Nakashima, J., Le Belle, J., Ohab, J., Kim, R., Liu, A., Smith, K.B.,
463 Groszer, M., Garcia, A.D., Sofroniew, M.V., Carmichael, S.T., et al. (2009). Pten
464 deletion in adult neural stem/progenitor cells enhances constitutive neurogenesis. J
465 Neurosci *29*, 1874-1886. 10.1523/JNEUROSCI.3095-08.2009.
466 24. Zhu, Y., Romero, M.I., Ghosh, P., Ye, Z., Charnay, P., Rushing, E.J., Marth, J.D., and
467 Parada, L.F. (2001). Ablation of NF1 function in neurons induces abnormal development
468 of cerebral cortex and reactive gliosis in the brain. Genes Dev *15*, 859-876.
469 10.1101/gad.862101.
470 25. Nelson, T., Pearce, D.A., and Kovacs, A.D. (2017). Lack of specificity of antibodies
471 raised against CLN3, the lysosomal/endosomal transmembrane protein mutated in
472 juvenile Batten disease. Biosci Rep *37*. 10.1042/BSR20171229.

473 26. Pontikis, C.C., Cotman, S.L., MacDonald, M.E., and Cooper, J.D. (2005).
474 Thalamocortical neuron loss and localized astrocytosis in the Cln3Deltaex7/8 knock-in
475 mouse model of Batten disease. Neurobiol Dis *20*, 823-836. 10.1016/j.nbd.2005.05.018.
476 27. Bosch, M.E., and Kielian, T. (2019). Astrocytes in juvenile neuronal ceroid lipofuscinosis
477 (CLN3) display metabolic and calcium signaling abnormalities. J Neurochem *148*, 612-
478 624. 10.1111/jnc.14545.
479 28. Zhong, Y., Mohan, K., Liu, J., Al-Attar, A., Lin, P., Flight, R.M., Sun, Q., Warmoes,
480 M.O., Deshpande, R.R., Liu, H., Jung, K.S., et al. (2020). Loss of CLN3, the gene
481 mutated in juvenile neuronal ceroid lipofuscinosis, leads to metabolic impairment and
482 autophagy induction in retinal pigment epithelium. Biochim Biophys Acta Mol Basis Dis
483 *1866*, 165883. 10.1016/j.bbadis.2020.165883.
484 29. Schultz, M.L., Tecedor, L., Lysenko, E., Ramachandran, S., Stein, C.S., and Davidson,
485 B.L. (2018). Modulating membrane fluidity corrects Batten disease phenotypes in vitro
486 and in vivo. Neurobiol Dis *115*, 182-193. 10.1016/j.nbd.2018.04.010.
487 30. Augustine, E.F., Beck, C.A., Adams, H.R., Defendorf, S., Vierhile, A., Timm, D.,
488 Weimer, J.M., Mink, J.W., and Marshall, F.J. (2019). Short-Term Administration of
489 Mycophenolate Is Well-Tolerated in CLN3 Disease (Juvenile Neuronal Ceroid
490 Lipofuscinosis). JIMD Rep *43*, 117-124. 10.1007/8904_2018_113.
491 31. El-Sitt, S., Soueid, J., Maalouf, K., Makhoul, N., Al Ali, J., Makoukji, J., Asser, B.,
492 Daou, D., Harati, H., and Boustany, R.M. (2019). Exogenous Galactosylceramide as
493 Potential Treatment for CLN3 Disease. Ann Neurol *86*, 729-742. 10.1002/ana.25573.
494 32. Petcherski, A., Chandrachud, U., Butz, E.S., Klein, M.C., Zhao, W.N., Reis, S.A.,
495 Haggarty, S.J., Ruonala, M.O., and Cotman, S.L. (2019). An Autophagy Modifier Screen
496 Identifies Small Molecules Capable of Reducing Autophagosome Accumulation in a
497 Model of CLN3-Mediated Neurodegeneration. Cells *8*. 10.3390/cells8121531.
498 33. Maalouf, K., Makoukji, J., Saab, S., Makhoul, N.J., Carmona, A.V., Kinarivala, N.,
499 Ghanem, N., Trippier, P.C., and Boustany, R.M. (2020). Exogenous Flupirtine as
500 Potential Treatment for CLN3 Disease. Cells *9*. 10.3390/cells9081872.
501 34. Centa, J.L., Jodelka, F.M., Hinrich, A.J., Johnson, T.B., Ochaba, J., Jackson, M., Duelli,
502 D.M., Weimer, J.M., Rigo, F., and Hastings, M.L. (2020). Therapeutic efficacy of
503 antisense oligonucleotides in mouse models of CLN3 Batten disease. Nat Med *26*, 1444-
504 1451. 10.1038/s41591-020-0986-1.
505 35. Bosch, M.E., Aldrich, A., Fallet, R., Odvody, J., Burkovetskaya, M., Schuberth, K.,
506 Fitzgerald, J.A., Foust, K.D., and Kielian, T. (2016). Self-Complementary AAV9 Gene
507 Delivery Partially Corrects Pathology Associated with Juvenile Neuronal Ceroid
508 Lipofuscinosis (CLN3). J Neurosci *36*, 9669-9682. 10.1523/JNEUROSCI.1635-16.2016.
509 36. Kleine Holthaus, S.M., Aristorena, M., Maswood, R., Semenyuk, O., Hoke, J., Hare, A.,
510 Smith, A.J., Mole, S.E., and Ali, R.R. (2020). Gene Therapy Targeting the Inner Retina
511 Rescues the Retinal Phenotype in a Mouse Model of CLN3 Batten Disease. Hum Gene
512 Ther *31*, 709-718. 10.1089/hum.2020.038.
513 37. Gray, S.J., Matagne, V., Bachaboina, L., Yadav, S., Ojeda, S.R., and Samulski, R.J.
514 (2011). Preclinical differences of intravascular AAV9 delivery to neurons and glia: a
515 comparative study of adult mice and nonhuman primates. Mol Ther *19*, 1058-1069.
516 10.1038/mt.2011.72.
517 38. Bey, K., Deniaud, J., Dubreil, L., Joussemet, B., Cristini, J., Ciron, C., Hordeaux, J., Le
518 Boulc'h, M., Marche, K., Maquigneau, M., Guilbaud, M., et al. (2020). Intra-CSF AAV9

519 and AAVrh10 Administration in Nonhuman Primates: Promising Routes and Vectors for
520 Which Neurological Diseases? Mol Ther Methods Clin Dev *17*, 771-784.
521 10.1016/j.omtm.2020.04.001.
522 39. Robel, S., Buckingham, S.C., Boni, J.L., Campbell, S.L., Danbolt, N.C., Riedemann, T.,
523 Sutor, B., and Sontheimer, H. (2015). Reactive astrogliosis causes the development of
524 spontaneous seizures. J Neurosci *35*, 3330-3345. 10.1523/JNEUROSCI.1574-14.2015.
525 40. Bourgeois, E.B., Johnson, B.N., McCoy, A.J., Trippa, L., Cohen, A.S., and Marsh, E.D.
526 (2014). A toolbox for spatiotemporal analysis of voltage-sensitive dye imaging data in
527 brain slices. PLoS One *9*, e108686. 10.1371/journal.pone.0108686.
528